Chemical Geology 362 (2013) 56–65

Contents lists available at ScienceDirect

Chemical Geology

journal homepage: www.elsevier.com/locate/chemgeo

Mass-independent fractionation of sulfur isotopes during broadband SO_2 photolysis: Comparison between ^{16}O- and ^{18}O-rich SO_2

Heather B. Franz [a,b,*], Sebastian O. Danielache [c], James Farquhar [b,d], Boswell A. Wing [e]

[a] Center for Research and Exploration in Space Science and Technology, NASA Goddard Space Flight Center, Greenbelt, MD 20771, USA
[b] Department of Geology, University of Maryland, College Park, MD 20742, USA
[c] Department of Environmental Science and Technology, Tokyo Institute of Technology, Yokohama, Japan
[d] Earth System Sciences Interdisciplinary Center, University of Maryland, College Park, MD 20742, USA
[e] Earth & Planetary Sciences and GEOTOP, McGill University, Montreal, Quebec H3A 2A7, Canada

ARTICLE INFO

Article history:
Accepted 24 July 2013
Available online 13 August 2013

Keywords:
Photochemistry
Sulfur dioxide
SO_2
Mass-independent fractionation
Mars
Martian

ABSTRACT

This paper describes a comparison of ultraviolet photolysis experiments undertaken with SO_2 (oxygen with isotopes at natural abundance levels) and $S^{18}O_2$ (^{18}O-substituted oxygen). Experiments were conducted in a closed photocell using a deuterium lamp (principally 190–235 nm) under pressure regimes (5–25 Torr) that produced optically thick conditions for $^{32}SO_2$ and variable optical depths for other isotopologues. The experiments, which were designed to examine the effects of intramolecular isotopic substitution of oxygen atoms on the S-MIF produced during UV photolysis of SO_2, reveal generally reduced sulfur fractionation for ^{18}O-rich SO_2 as compared to ^{16}O-rich SO_2. Model shielding calculations were undertaken using spectra that were shifted due to changes in rotational and vibrational energy levels. The model calculations suggest that processes in addition to rotational and vibrational shifts in absorption spectra play a role in the experimentally produced isotope effects. Such additional processes may include differences in primary photoexcitation arising from smaller peak-to-valley amplitudes for fine structure of ^{18}O-rich SO_2 absorption spectra or an isotopically selective process associated with transitions between excited states.

1. Introduction

The past few decades have witnessed extensive growth in the application of sulfur isotope systematics to investigate processes of interest to both planetary and cosmochemical studies. The link between the rise of oxygen in the Earth's atmosphere and oceans ~2.4 Ga that has been termed the "Great Oxidation Event" (Holland, 2006) and a corresponding attenuation of mass-independent sulfur isotopic fractionation (S-MIF) observed in Archean samples (Farquhar et al., 2000a) has provided focus for models of atmospheric evolution. Laboratory experiments have indicated that S-MIF is produced in gas-phase ultraviolet (UV) photochemistry of sulfur-bearing molecules, including SO_2, H_2S, and CS_2 (Zmolek et al., 1999; Farquhar et al., 2000c, 2001), and many of the specific causes of this chemistry remain to be understood. Comparison of sulfur isotope fractionation produced by laboratory photochemistry experiments and the S-MIF signals observed in the ancient terrestrial rock record as well as in meteorites provides compelling evidence for a cause-and-effect relationship (e.g., Farquhar et al., 2000b, 2000c, 2001, 2007a). If this relationship were fully characterized, it could provide constraints on the chemical and physical compositions of the respective planetary atmospheres at the times the anomalous signals were generated. For example, the abundance of SO_2 in the martian atmosphere is critical to its potential role as a greenhouse gas early in Mars' history (e.g., Postawko and Kuhn, 1986; Halevy et al., 2007; Johnson et al., 2008, 2009; Tian et al., 2010). Such characterization requires determination of the mechanism responsible for producing the observed fractionation.

Possible mechanisms for generating the S-MIF signal include shielding effects within the gas and isotopologue-specific absorption or kinetics. Shielding refers to a process in which molecules located between the radiation source and the reaction site absorb radiation and limit the availability of radiation for chemistry at the reaction site (Bally and Langer, 1982). Self-shielding refers to the shielding of radiation by a molecule on other molecules with the same isotopic configuration (i.e., isotopomers). Mutual shielding refers to the shielding of radiation by a molecule on other molecules with different isotopic (i.e., isotopologues) or chemical compositions. Both aspects of shielding are important during photolysis of SO_2 in experiments like those described here and in nature. In this paper, for clarity, the term "shielding" is used to describe a specific phenomenon due to the column density of the absorbing species, resulting in saturation of absorption by a given isotopologue and disproportionate enrichment of photochemical products formed from other isotopologues.

* Corresponding author at: NASA/GSFC Code 699, Building 33, Room F109A, Greenbelt, MD 20771, USA. Tel.: +1 301 614 5463; fax: +1 301 614 6406.
E-mail address: heather.b.franz@nasa.gov (H.B. Franz).

0009-2541/$ – see front matter © 2013 Elsevier B.V. All rights reserved.
http://dx.doi.org/10.1016/j.chemgeo.2013.07.021

The concept of shielding has been invoked most frequently to explain mass-independent fractionations due to photochemical processes. Lyons (2007) argued that shielding during SO_2 photolysis is theoretically predicted to generate S-MIF and may explain the signatures observed in Archean samples (Farquhar et al., 2000a, 2007b). Mass-independent fractionation may also result from variations in absorption cross-section that favor promotion of certain isotopologues to excited states over others (e.g., Zmolek et al., 1999; Danielache et al., 2008, 2012). These types of effects result in variation in the isotopologue-specific photolysis rates even in an optically thin atmosphere (c.f. Schmidt et al., 2011, 2012). Danielache et al. (2008) reported spectroscopic measurements of the UV absorption spectrum of SO_2, noting rich vibrational structure and complex shifts in position, width, and height of peaks with isotopic substitution. These examples represent potential mechanisms for producing variations in total integrated absorption among the isotopologues independently of their relative abundances.

A third pathway for mass-independent fractionation is associated with differences in the rates at which different excited state isotopologues react, either during transitions from one state to another state or along a reaction path involving dissociation or reaction with other species (e.g., Thiemens and Heidenreich, 1983; Thiemens et al., 2012). Isotopologue-dependent variations in lifetime of excited states produced upon photon absorption would fall under this category (Okabe, 1978).

All of these mechanisms are thought to play a role in experiments (e.g., Farquhar et al., 2001; Masterson et al., 2011) and in nature (e.g., Farquhar et al., 2000a, 2000b; Savarino et al., 2003; Ueno et al., 2009), but questions remain about the relative importance of each in generating the observed S-MIF (Lyons, 2007; Danielache et al., 2008; Ueno et al., 2009; Masterson et al., 2011). Here we describe experiments designed to examine the photochemical effects on ^{18}O-substituted SO_2 gas using a deuterium lamp source, which emits broadband radiation from 180 to 360 nm. Experiments with natural abundance (^{16}O-rich) SO_2 provided a baseline for comparison of photochemical effects of the broadband source with those of previous experiments using other types of UV sources. The experiments with ^{18}O-rich SO_2 were designed to provide potential clues to the mechanism responsible for producing the S-MIF signal. A model was also devised, based on theoretical predictions of shifts in absorption spectra for heavy SO_2 isotopologues, in an attempt to examine whether changes in the absorption spectra arising from different rotational and vibrational energies associated with ^{18}O substitution of sulfur dioxide would produce similar magnitude changes in the isotopic compositions as observed in the experiments. Hereafter, the term "SO_2" is used to denote SO_2 with natural abundance of oxygen isotopes (i.e., ^{16}O-rich SO_2) and "$S^{18}O_2$" to denote ^{18}O-rich SO_2.

2. Experimental methods

The experiments described here were performed with a 300-watt Oriel-66136 deuterium source operated at 2 A, generating broadband UV radiation from 180 to 360 nm. The spectrum of the deuterium lamp from 180 to 300 nm was measured at the NASA Goddard Space Flight Center with an Acton Research Corporation UV spectrometer, comprising a monochromator and reflectometer connected to a photomultiplier tube. To replicate the conditions of the photolysis experiments, the deuterium lamp was placed with its window in room air, adjacent to the MgF_2 window of the spectrometer chamber. A fused silica filter in front of the detector mimicked the attenuation effects of the photocell window during the experiments. The lamp spectrum from 300 to 390 nm was extrapolated based on data provided by Oriel.

Each experiment was run with one of two glass reaction cells of 4-mm wall thickness: a cylindrical cell with inner diameter of 1.9 cm, length of 44 cm, and volume of 164.8 cm^3, and a spherical cell with diameter of 10.9 cm and volume of 536.1 cm^3. Each reaction cell was epoxy-sealed to a 4-mm fused silica window with diameter of 2.3 cm. The reaction cell was connected to a modular photolysis sampling manifold constructed from glass and flexible stainless steel tubing.

Since UV radiation is known to damage epoxy, we focused the light beam so that it only filled ~3/4 of the window. In addition, leak tests were conducted before and after each experiment. Before each experiment, the photocell was heated with a heat gun and evacuated to <1 mTorr, then isolated from vacuum. Gas pressures were monitored for 6–24 h and the windows were replaced if pressure increased beyond the reported resolution of the manometer (0.01 mTorr). After each experiment, gases in the cell were condensed into a cold finger cooled with liquid nitrogen. Final pressures after condensation were usually within uncertainty of the manometer's baseline, implying that the net reaction

$$3SO_2 \rightarrow S + 2SO_3 \quad (1)$$

encompasses the chemical transformation that occurred during the experiments. This behavior also provided a check on the integrity of the epoxy seal since a leak would have led to the introduction of non-condensable gases under liquid nitrogen and non-zero pressures in the photocell. These were not noted in any of the experiments reported here.

Commercial SO_2 gases were purchased from Alfa Aesar (99% purity - SO_2 with natural abundances) and Icon Isotopes (97% ^{18}O substituted SO_2). The $\delta^{33}S$, $\delta^{34}S$, and $\delta^{36}S$ values of the starting SO_2 gas are −3.67‰, −7.06‰, and −13.49‰ relative to V-CDT. The $\delta^{33}S$, $\delta^{34}S$, and $\delta^{36}S$ values of the starting $S^{18}O_2$ gas are −0.88‰, −1.74‰ and −3.43‰ relative to V-CDT. For each experiment, SO_2 gas was introduced into the evacuated manifold to achieve an experimental pressure of approximately 5–25 Torr. The SO_2 was then cryogenically purified with liquid nitrogen. A small amount of non-reacted SO_2 was preserved at the beginning of each experiment for measurement of the initial sulfur isotopic composition. The remainder was isolated in the reaction cell, which was placed with its fused silica window adjacent to the deuterium lamp aperture. The entire reaction cell was wrapped with aluminum foil to isolate the lighting conditions inside the cell from the ambient laboratory environment.

After the SO_2 in the reaction cell was irradiated for ~2 to 4.5 h, the products (including elemental sulfur and sulfur trioxide, SO_3) and residual SO_2 were extracted and processed using standard laboratory methods (Farquhar et al., 2001; Johnston et al., 2006). The preserved initial SO_2 and the final SO_x (assumed to be SO_3 or possibly sulfuric acid due to its hydration reaction) were converted to sulfate by reaction with 30% hydrogen peroxide solution at room temperature. The resulting sulfuric acid was extracted with Milli-Q water and then precipitated as barium sulfate by the addition of several drops of 10% barium chloride solution. The barium sulfate was rinsed with Milli-Q water and dried in a 90 °C oven prior to reduction. The dried barium sulfate was reduced in a boiling flask with 25 mL of a solution prepared from 12 N hydrochloric, 48% hydriodic, and 50% hypophosphorous acids (Thode et al., 1961). The boiling flask was connected to the lower adapter of a distillation apparatus that was actively purged with nitrogen gas. The solution was heated to ~85 °C for approximately 3 h, reducing the barium sulfate to H_2S. After passing through a Milli-Q water trap, purified H_2S was carried through a centrifuge tube containing 14 mL of 0.1 M zinc acetate solution, where it reacted to form zinc sulfide. Dropwise addition of 0.2 M silver nitrate solution after the distillation process converted the zinc sulfide to silver sulfide, Ag_2S. After allowing at least several hours for the conversion to complete, the resulting precipitate was filtered on a 0.2 μm cellulose filter and rinsed with 150 mL of Milli-Q water, washed with 15 mL of 0.1 M ammonium hydroxide solution to remove excess silver ions, then rinsed with an additional 150 mL of Milli-Q water. Ag_2S was transferred from the filter paper to aluminum foil packets that had been cleaned with ethanol and dried overnight in a 90° C oven.

A similar method was used for the reduction of product elemental sulfur, which was extracted from the reaction cell with carbon

tetrachloride and evaporated to dryness in a double-necked boiling flask with septum seal. The flask was connected to the lower adapter of a distillation apparatus purged with nitrogen gas. Chromium (II) reduction solution (CRS) was prepared in a nitrogen atmosphere by overnight reaction of chromium (III) chloride in a solution of 0.5 N HCl and zinc metal. Fifteen mL of CRS and 15 mL of 5 N HCl were injected through the septum into the boiling flask containing the elemental sulfur sample, with nitrogen flowing through the distillation apparatus. Solutions were heated to ~60 °C for approximately 3 h, generating H_2S that was captured and converted to Ag_2S as described above, with one exception. In some experiments, particularly when the irradiation duration was relatively short, the product yield of elemental sulfur was too low for cellulose filtering of the Ag_2S. In these cases, the Ag_2S was instead purified by centrifugation and washing with Milli-Q water and ammonium hydroxide solution.

Ag_2S was converted to SF_6 by reaction with 250 μmol of fluorine gas in a nickel reaction vessel at 250 °C for 8 h. The SF_6 was subsequently condensed from the residual F_2 into a trap cooled with liquid nitrogen. Excess F_2 was passivated by reaction with KBr salt. Replacement of the liquid nitrogen coolant on the trap with ethanol slush at −115 °C allowed distillation of the SF_6 from the trap into the liquid-nitrogen-cooled injection loop of a gas chromatograph (GC). The SF_6 was purified by a 1/8-inch diameter, 6-foot long Molecular Sieve 5A GC column, followed by a 1/8-inch diameter, 12-foot long Haysep-Q™ GC column. Both columns were held at 50 °C, with helium carrier gas flow rate of 20 mL/min. After its elution from the GC column, the SF_6 was captured in spiral glass traps cooled with liquid nitrogen, then transferred to the bellows of a Thermofinnigan MAT 253 dual-inlet gas source mass spectrometer. The sulfur isotopic composition of the SF_6 was measured by monitoring SF_5^+ ion beams at m/z of 127, 128, 129, and 131 Da. Results of the experiments were renormalized with respect to the initial SO_2 isotopic composition to facilitate understanding of the photochemical fractionation effects. Isotopic compositions are given in conventional delta notation:

$$\delta^{34}S = 1000\left[\left(^{34}S/^{32}S\right)_{sample}/\left(^{34}S/^{32}S\right)_{ref}-1\right] \quad (2)$$

$$\delta^{33}S = 1000\left[\left(^{33}S/^{32}S\right)_{sample}/\left(^{33}S/^{32}S\right)_{ref}-1\right] \quad (3)$$

$$\delta^{36}S = 1000\left[\left(^{36}S/^{32}S\right)_{sample}/\left(^{36}S/^{32}S\right)_{ref}-1\right] \quad (4)$$

$$\Delta^{33}S = \delta^{33}S - 1000\left[\left(1+\delta^{34}S/1000\right)^{0.515}-1\right] \quad (5)$$

$$\Delta^{36}S = \delta^{36}S - 1000\left[\left(1+\delta^{34}S/1000\right)^{1.90}-1\right]. \quad (6)$$

Estimated 1σ uncertainties based on repeated measurements of IAEA reference materials in this laboratory are generally better than 0.15‰, 0.008‰, and 0.15‰ for $\delta^{34}S$, $\Delta^{33}S$, and $\Delta^{36}S$, respectively. However, the analytical uncertainties in mass spectrometric measurements for specific values are reported when they exceed these values, to represent more accurately the larger uncertainties encountered in measuring isotope ratios of extremely small quantities of analyte.

3. Experimental results

Table 1a presents the data collected from the SO_2 and $S^{18}O_2$ photolysis experiments, with uncertainties given in Table 1b. The data as shown in Table 1a represent fractionation with respect to the sulfur isotopic composition of the initial gas. The corresponding uncertainties in Table 1b include error propagation from the renormalization of raw data with respect to the initial gas. The data indicate reduced magnitude of fractionation for the experiments with ^{18}O-rich SO_2 as compared to ^{16}O-rich SO_2. Products and residual gas from the $S^{18}O_2$ experiments show both smaller delta values for each sulfur isotope and smaller deviations from mass-dependent behavior, quantified as $\Delta^{33}S$ and $\Delta^{36}S$.

The measured $\delta^{34}S$ of elemental sulfur from the $S^{18}O_2$ experiments ranges from 92.05 ± 0.15‰ to 114.89 ± 0.15‰ (average 104.38 ± 4.32‰, standard error of the mean). In comparison, the SO_2 experiments yield product elemental sulfur with $\delta^{34}S$ ranging from 167.81 ± 0.15‰ to 177.22 ± 0.11‰ (average 172.76 ± 1.68‰). On average, the difference in $\delta^{34}S$ for the SO_2 and $S^{18}O_2$ experiments ($SO_2 - S^{18}O_2$) is 68.38 ± 4.64‰. The residual SO_x compositions generally indicate a lower range of fractionation for the $S^{18}O_2$ experiments than for those performed with ^{16}O-rich SO_2. The residual SO_x from $S^{18}O_2$ shows $\delta^{34}S$ of −1.25 ± 0.15‰ to −2.48 ± 0.15‰ (average −2.03 ± 0.22‰). For the ^{16}O-rich SO_2 experiments, residual SO_x shows $\delta^{34}S$ of −1.37 ± 0.15‰ to −5.56 ± 0.15‰ for (average −3.04 ± 0.93‰). On average, the difference in $\delta^{34}S$ of residual SO_x for the SO_2 and $S^{18}O_2$ experiments ($SO_2 - S^{18}O_2$) is −1.01 ± 0.95‰.

Deviation from mass-dependent fractionation is illustrated on plots of $\Delta^{33}S$ versus $\delta^{34}S$ and $\Delta^{36}S$ versus $\delta^{34}S$ in Fig. 1. Fig. 1(a) shows $\Delta^{33}S$ versus $\delta^{34}S$ for both residual SO_2 and product elemental sulfur, while Fig. 1(b) shows a detailed perspective of the residual gas data. Elemental sulfur has $\Delta^{33}S$ values of 8.33 ± 0.05‰ to 16.30 ± 0.05‰ (average 13.25 ± 1.38‰) for experiments with $S^{18}O_2$ and 16.56 ± 0.05‰ to 23.19 ± 0.05‰ (average 18.60 ± 1.17‰) for experiments with SO_2. Fig. 1(b) shows $\Delta^{33}S$ for residual gas of −0.02 ± 0.05‰ to −0.25 ± 0.05‰ (average −0.15 ± 0.04‰) for $S^{18}O_2$ and −0.10 ± 0.04‰ to −0.52 ± 0.05‰ (average −0.27 ± 0.08‰) for SO_2 experiments. As expected from mass balance considerations, Fig. 1(a) shows that the $\Delta^{33}S$ values for elemental sulfur lie above the x-axis, which represents mass-dependent fractionation, while the residual gas data in Fig. 1(b) lies below the x-axis.

Similar data for $\Delta^{36}S$ are shown in Fig. 1(c) and (d). Fig. 1(c) displays $\Delta^{36}S$ versus $\delta^{34}S$ for both residual SO_2 and product elemental sulfur, while Fig. 1(d) shows a detailed perspective of the residual gas data. The $\Delta^{36}S$ for elemental sulfur ranges from −21.33 ± 2.16‰ to −41.86 ± 0.48‰ (average −33.59 ± 4.03‰) for experiments with $S^{18}O_2$ and −41.09 ± 0.38‰ to −48.63 ± 0.43‰ (average −43.47 ± 1.37‰) for experiments with SO_2. As detailed in Fig. 1(d), $\Delta^{36}S$ for residual gas ranges from −0.20 ± 0.22‰ to 0.67 ± 0.22‰ (average 0.18 ± 0.22‰) for $S^{18}O_2$ and 0.06 ± 0.23‰ to 0.35 ± 0.21‰ (average 0.19 ± 0.23‰) for SO_2 experiments. Fig. 1(c) shows that the $\Delta^{36}S$ for elemental sulfur lies below the x-axis that defines the mass-dependent fractionation baseline, while the residual gas data illustrated in Fig. 1(d) lie primarily above the baseline.

It is clear from Fig. 1(a) through (d), which graphically displays the differences in sulfur fractionation between the $S^{18}O_2$ and SO_2 experiments, that the elemental sulfur produced during photolysis of $S^{18}O_2$ is less fractionated with respect to the initial gas than that produced during experiments with SO_2. It is also evident from the figures that the experimental products do not exhibit mass-dependent isotopic composition. The $\Delta^{33}S$ and $\Delta^{36}S$ of the elemental sulfur products do not show strong correlation with $\delta^{34}S$, but are clustered within small ranges of $\delta^{34}S$ for the ^{18}O-rich and ^{16}O-rich SO_2 samples. In addition, the clusters of products for ^{18}O-rich and ^{16}O-rich SO_2 samples display similar relationships for $\Delta^{33}S/\delta^{34}S$ and $\Delta^{36}S/\delta^{34}S$ and have a common $\Delta^{36}S/\Delta^{33}S$ of approximately −2.4.

Yields of elemental sulfur (calculated as S_8) scaled in approximately linear fashion with reaction duration, ranging from <0.1% for 2-hour durations and ~0.5% for experiments of ~4.5 h. However, there was no clear correlation between either experiment duration or starting SO_2 pressure and $\Delta^{33}S$ or $\Delta^{36}S$ of the reaction products. Due to the low photolysis yield, the probability of collision between photolytically-produced O and the major species SO_2 is much greater than the

Table 1a
Sulfur isotopic data from photolysis experiments presented as per mil deviation from isotopic composition of initial gas and yields of elemental sulfur (S_8).

	Conditions			*Residual SO_x*			*Product elemental sulfur*		
	P (Torr)	Duration (h)	Yield (%)	$\delta^{34}S$	$\Delta^{33}S$	$\Delta^{36}S$	$\delta^{34}S$	$\Delta^{33}S$	$\Delta^{36}S$
SO_2	5.4	4.7	0.57	−5.04	−0.52	0.35	175.33	23.19	−48.63
	25.7	4.5	0.41	−1.37	−0.10	0.10	177.22	17.40	−43.74
	21.2	2.0	0.07	−1.66	−0.13	0.15	167.81	16.56	−41.09
	17.8	2.0	0.08	−1.57	−0.18	0.06	170.41	17.92	−41.37
	18.6	4.5	0.54	−5.56	−0.40	0.30	173.03	17.93	−42.54
$S^{18}O_2$	23.3	2.0	0.02	−1.88	−0.18	0.01	114.89	15.23	−41.44
	16.3	2.0	0.05	−2.38	−0.25	0.67	113.05	16.30	−41.86
	25.6	4.5	0.44	−2.16	−0.02	−0.20	103.43	8.33	−35.96
	13.7	2.0	0.02	−1.25	−0.12	0.24	92.05	12.56	−21.33
	19.3	2.0	0.03	−2.48	−0.19	0.19	98.47	13.82	−27.37
				Averages					
				$\delta^{34}S$	$\Delta^{33}S$	$\Delta^{36}S$	$\delta^{34}S$	$\Delta^{33}S$	$\Delta^{36}S$
SO_2				−3.04 ± 0.15	−0.27 ± 0.05	0.19 ± 0.22	172.76 ± 0.15	18.60 ± 0.05	−43.47 ± 0.38
$S^{18}O_2$				−2.03 ± 0.15	−0.15 ± 0.05	0.18 ± 0.25	104.38 ± 0.15	13.25 ± 0.06	−33.59 ± 1.03

probability of collision with any minor species produced in the cell, including collision with O to form O_2. A review of the relative reaction rates for relevant species, compiled in Johnson et al. (2009), also suggests that reaction of O with SO_2 proceeds more rapidly than reaction with O to form O_2. As a result, the buildup of O_2 in the cell should be negligible, and O molecules generated by photolysis predominantly react with SO_2 to form SO_3.

4. Discussion

4.1. SO_2 absorption spectrum

SO_2 exhibits a complex absorption spectrum in the near UV as well as vacuum UV regions, as shown in Fig. 2. According to Okabe (1978), there are three main SO_2 absorption regions in the UV. A very weak absorption at 340–390 nm and a moderate absorption at 240–340 nm are characterized by photoexcitation resulting in fluorescence, phosphorescence, or self-quenching products of SO_2, SO and SO_3. A strong absorption system at 180–235 nm is attributed to competition between fluorescence, which predominates at wavelengths longer than 219.2 nm, and predissociation leading to the production of SO, predominating at wavelengths shorter than 219.2 nm. Photodissociation of sulfur monoxide to elemental sulfur is also attributed to predissociation near 200 nm (e.g., Speth et al., 1998; Archer et al., 2000). Details concerning the excited states of SO_2 following UV photoabsorption are discussed elsewhere (e.g., Okabe, 1978; Wu et al., 2000; Xie et al., 2000; Lyons, 2007; Ran et al., 2007) and will not be repeated here.

Table 1b
Uncertainties (1σ) in sulfur isotopic data from photolysis experiments.

	Residual SO_x			*Product elemental sulfur*		
	$\delta^{34}S$	$\Delta^{33}S$	$\Delta^{36}S$	$\delta^{34}S$	$\Delta^{33}S$	$\Delta^{36}S$
SO_2	±0.15	±0.05	±0.21	±0.15	±0.05	±0.43
	±0.15	±0.04	±0.22	±0.15	±0.05	±0.36
	±0.15	±0.05	±0.22	±0.15	±0.05	±0.38
	±0.15	±0.05	±0.23	±0.15	±0.05	±0.35
	±0.15	±0.04	±0.21	±0.15	±0.05	±0.39
$S^{18}O_2$	±0.15	±0.04	±0.24	±0.15	±0.06	±0.33
	±0.15	±0.05	±0.22	±0.15	±0.05	±0.48
	±0.15	±0.04	±0.22	±0.15	±0.05	±0.30
	±0.15	±0.05	±0.37	±0.15	±0.08	±2.16
	±0.15	±0.05	±0.22	±0.15	±0.07	±1.85

Because of the spectrum of the deuterium source used, these experiments principally probed the absorption system from 180 to 235 nm, with some longer wavelength contributions. However, Whitehill and Ono (2012) demonstrated in similar experiments that contributions from the band at 240–340 nm are very minor. Fig. 2 displays the absorption spectrum of SO_2 as well as the normalized deuterium lamp spectrum as a function of wavelength. A second deuterium lamp spectrum, generated from a different source with its output inside the spectrometer vacuum chamber, is also shown in the figure for comparison. Comparison of these two spectra suggests that absorption below ~190 nm principally by lenses and to a lesser extent by air, which may introduce additional structure to the spectrum due to absorption by the Schumann–Runge bands, prevents a portion of radiation at the shortest wavelengths from reaching the reaction zone inside the photocell. The net effects of this short wavelength absorption and the emission properties of the deuterium source are to yield the most substantial radiation in the 190–235 nm wavelength window during the experiments.

Numerous reactions of ground state and excited state SO_2 and subsequent products characterize the reaction network in the wavelength range of interest. Since we are concerned primarily with the source of the observed elemental sulfur that bears large S-MIF signatures, it is most instructive to consider the specific reactions responsible for liberation of sulfur atoms from SO_2, rather than to list all possible reactions that may have occurred in the cell. There are two general pathways through which elemental sulfur may be photolytically produced (Okabe, 1978). The first is successive photolysis of SO_2 and SO at wavelengths in the window from ~200–220 nm:

$$SO_2 + h\nu \rightarrow SO + O \quad (7)$$

$$SO + h\nu \rightarrow S + O. \quad (8)$$

A second pathway involves the absorption of light in the wavelength windows from 240 to 340 nm and from 340 to 390 nm:

$$^{*}SO_2 + SO_2 \rightarrow SO_3 + SO, \quad (9)$$

where $^{*}SO_2$ indicates excited-state SO_2, followed by photolysis of the resulting SO as above. Given the experimental conditions and the fact that SO_2 absorption in the bands at 240–340 nm and 340–390 nm is much weaker than absorption at 190–235 nm, it is most probable that the elemental sulfur formed in the photocell was the product of reactions (7) and (8). Back reactions of elemental sulfur with oxygen or oxidized sulfur species may occur, contributing to the low experimental yields, but sulfur oxidation reactions are not known to introduce

Table 2
Linear fit parameters for red-shifting of isotopologue spectra relative to $^{32}SO_2$. The slope and the origin are given in units of cm^{-1}.

	$^{17}O^{32}S^{16}O$	$^{18}O^{32}S^{16}O$	$^{17}O^{32}S^{17}O$	$^{18}O^{32}S^{18}O$	$^{18}O^{33}S^{18}O$	$^{18}O^{34}S^{18}O$	$^{18}O^{36}S^{18}O$
Slope	0.006092	0.011745	0.00954	0.0219	0.04306	0.04722	0.05496
Origin	−256.28	−485.53	−391.21	−904.55	−1817.34	−1944.74	−2182.45

anomalous isotopic fractionation and should not have affected the S-MIF of the elemental sulfur product.

4.2. Investigating the source of the observed S-MIF through modeling based on synthetic $^{32,33,34\&36}S^{18}O_2$ spectra

4.2.1. Model description

Ran et al. (2007) computed theoretical absorption spectra for $^{32}SO_2$, $^{33}SO_2$, $^{34}SO_2$, and $^{36}SO_2$ in the wavelength band from 180 to 220 nm based on a quantum mechanical approach. Those authors noted monotonic shifts in positions of spectral features with isotopic substitution in this region, which is dominated by the (1, ν_2, 0) and (1, ν_2, 2) bending mode progressions. Lyons (2007) applied the shifts in vibronic features for the (1, ν_2, 2) progression computed by Ran et al. (2007) to the measured $^{32}SO_2$ spectrum of Freeman et al. (1984) to investigate the potential for isotopic fractionation during photolysis of $^{32}SO_2$, $^{33}SO_2$, $^{34}SO_2$, and $^{36}SO_2$ at these wavelengths.

An approach similar to that of Lyons (2007) was employed in the current study to investigate potential S-MIF effects due to differences in absorption spectra, but extended to include substitution of oxygen as well as sulfur isotopes. Simulated absorption spectra for various SO_2 isotopologues were generated by red-shifting the measured $^{32}SO_2$ spectrum of Danielache et al. (2008) using shifting parameters (Table 2) taken from theoretical calculations of Tokue and Nanbu (2010), where SO_2 spectra for several oxygen and sulfur isotopologues were calculated by means of wavepacket propagation. These parameters represent the change in vibrational energy of each isotopologue in the excited C^1B_2–X^1A_1 band. The main differences between our model and Lyon's model reside in the improved shifting parameters calculated by Tokue and Nanbu and in the employed $^{32}SO_2$ spectra. The decision to use the spectra published by Danielache et al. (2008) was made because this is the

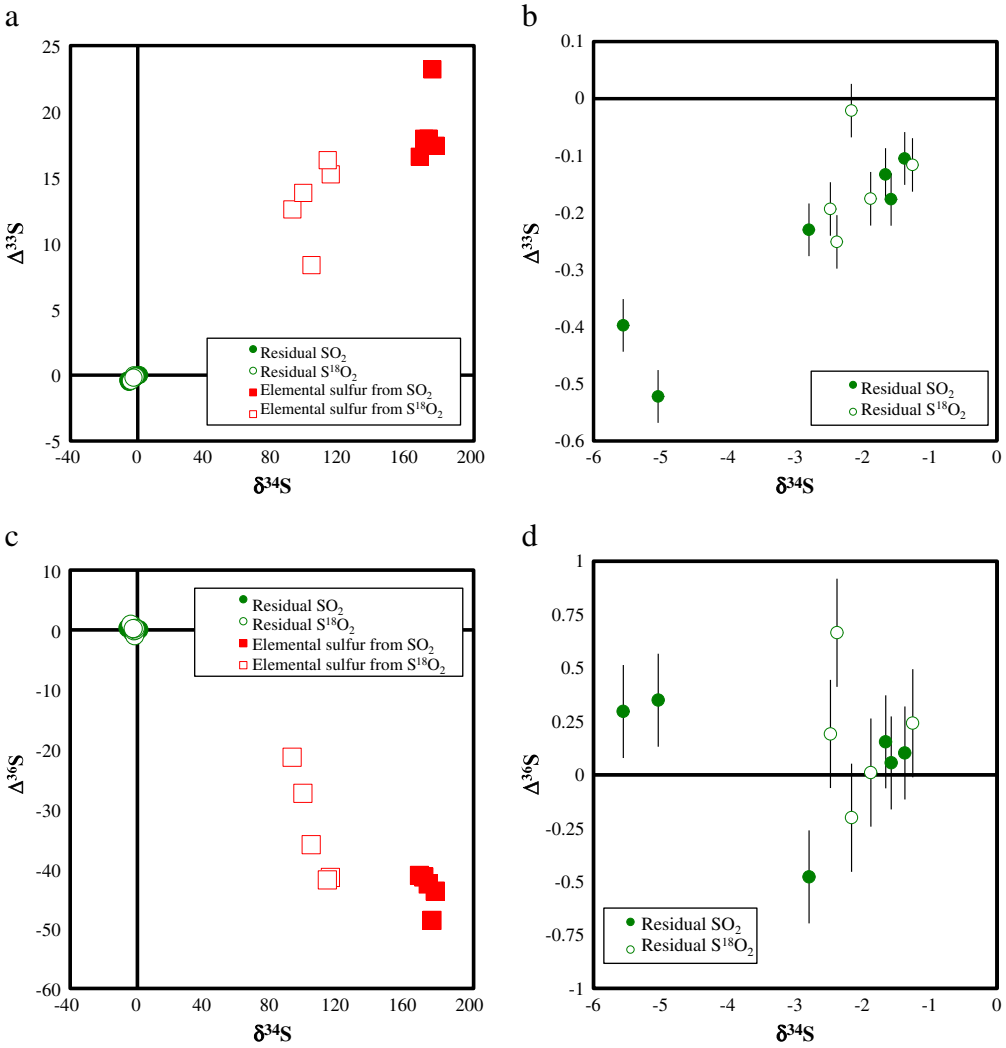

Fig. 1. Isotopic composition of products and residues of photolysis experiments. Results are reported with respect to the initial gas composition. If 2σ error bars are not visible, they are smaller than the symbols. (a) $\Delta^{33}S$ vs. $\delta^{34}S$ for residual gas and elemental sulfur product. (b) $\Delta^{33}S$ vs. $\delta^{34}S$ for residual gas. (c) $\Delta^{36}S$ vs. $\delta^{34}S$ for residual gas and elemental sulfur product. (d) $\Delta^{36}S$ vs. $\Delta^{34}S$ for residual gas.

only available $^{32}SO_2$ data set (as opposed to the natural abundance measurement of Freeman et al., 1984). In addition, the isotopically enriched spectra of Danielache et al. (2008) was selected over the high-resolution spectra of Freeman et al. (1984) due to the higher accuracy of calculated absorption cross-sections and the observation that even a 100 times higher resolution does not present any discernible difference in the spectral features (Fig. S1).

The validity of the model resides in the ability to create $^{3x}S^{18}O_2$ spectra from measured $^{32}SO_2$ data and theoretically-calculated shifting parameters. The shifting parameters take into account changes in vibrational energies for each isotopologue down the progression and, as presented in Fig. S2, comparison with available experimental data shows undisputable reproducibility. Isotopic effects on the absorption intensity of each rovibrational feature and changes in the population density of the rotational lines are likely to affect the spectra of heavier isotopologues. These effects alter the waveform of the spectra with respect to the original $^{32}SO_2$ spectrum and since they are not taken into account in the model, these sources of error must be quantified. Figs. S3 (a) and (b) show that sulfur isotope effects for the isotopologues of ^{16}O are similar to those of ^{18}O. The ^{18}O isotopologues are more red-shifted than their ^{16}O counterparts, but the magnitude of these shifts is ~10 cm^{-1} at J values above 20, representing an upper limit to how the overlapping of heavily populated rotational lines from multiple vibrational progressions may affect the resulting spectra. Additional confirmation is obtained by comparing calculated and measured shifting parameters for $^{32}S^{16}O_2$ and $^{32}S^{18}O_2$ (Fig. S4). The comparison of these data sets predicts minimal change to the waveform due to isotopic effects.

Given the extent to which the synthetic spectra are capable of representing realistic $^{3x}S^{18}O_2$ spectra, as discussed above, we expect the largest source of isotopic effects to reside in the overlapping of the shifted spectra toward a region of the spectrum where actinic flux is slightly higher (Figs. S5 to S7). It is important to note that this effect operates in the specific experimental conditions of our experiment. Based on the above assessment we proceeded to calculate a number of models with different opacity term conditions.

The following mathematical formulation has been slightly modified from that of Danielache et al. (2008). In Eqs. (10) through (13), x = 16 or 18 and y = 33, 34, or 36. The total absorption for each isotopologue was integrated over the wavelength window of 190–220 nm, analogous to our experimental conditions, resulting in relative band intensities given by

$$J_{x\_y\_x} = \frac{\int_{190}^{220} F_0(\lambda)\sigma_{x\_y\_x}(\lambda)e^{-\tau_{x\_y\_x}(\lambda)}d\lambda - \int_{190}^{220} F_0(\lambda)\sigma_{x\_Nat\_x}(\lambda)e^{-\tau_{x\_Nat\_x}(\lambda)}d\lambda}{\int_{190}^{220} F_0(\lambda)\sigma_{x\_Nat\_x}(\lambda)e^{-\tau_{x\_Nat\_x}(\lambda)}d\lambda}. \quad (10)$$

In this expression, for example, $\sigma_{16\_33\_16}$ would refer to the absorption cross-section for $^{33}S^{16}O_2$ and Nat indicates the natural distribution of the sulfur isotopes. $F_0(\lambda)$ is the relative incident radiation intensity as measured for the deuterium lamp source, and $\tau_{x\_y\_x}(\lambda)$ is the optical depth for each isotopologue at a given experimental condition. Since the elemental sulfur products formed primarily on the window in front of the photocell, the optical depth was simulated as an overhead column with no real physical units of distance. Photodissociation quantum yield was assumed to be 1 in all cases (i.e., no effect arising from subsequent state-to-state transformations). Fractionation constants were derived from the integrated absorptions as follows:

$$\varepsilon_{x\_y\_x} = 1000 \times ln\left[\frac{\int_{190}^{220} F_0(\lambda)\sigma_{x\_y\_x}(\lambda)e^{-\tau_{x\_y\_x}(\lambda)}d\lambda}{\int_{190}^{220} F_0(\lambda)\sigma_{x\_32\_x}(\lambda)e^{-\tau_{x\_32\_x}(\lambda)}d\lambda}\right]. \quad (11)$$

To assess predicted deviations from mass-dependent fractionation, the following relationships were employed:

$$\Delta^{33}_{x\_33\_x} = \varepsilon_{x\_33\_x} - 1000 \times ln\left[\left(\frac{\varepsilon_{x\_34\_x}}{1000}+1\right)^{0.515} - 1\right] \quad (12)$$

$$\Delta^{36}_{x\_36\_x} = \varepsilon_{x\_36\_x} - 1000 \times ln\left[\left(\frac{\varepsilon_{x\_34\_x}}{1000}+1\right)^{1.90} - 1\right]. \quad (13)$$

4.2.2. Model results

Results for relative band intensities as percent deviations from the $^{32}S^{x}O_2$ band (Eq. (10)) are presented in Tables 3a and 3b, along with predictions for fractionation constants and mass-independent behavior. The model predicted significant enrichments in all of the minor sulfur

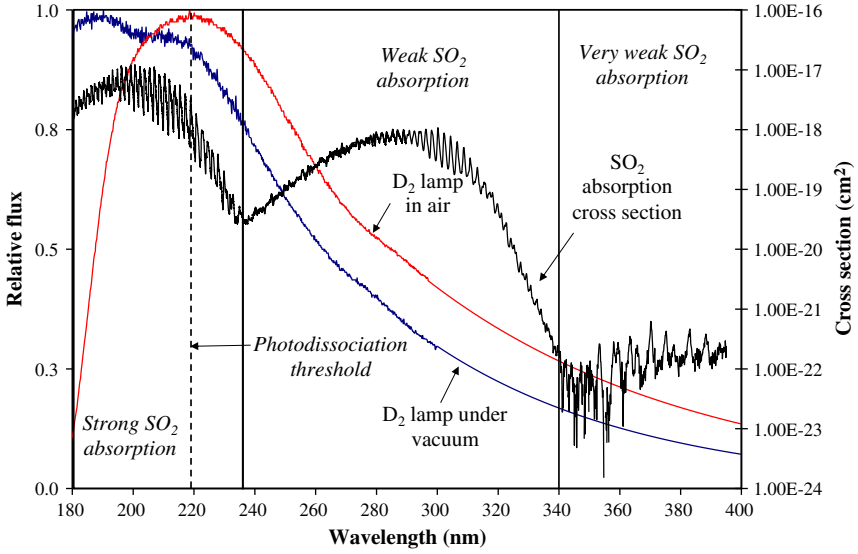

Fig. 2. Deuterium lamp spectrum and SO_2 absorption spectrum. The lamp spectrum in air is representative of the conditions for the experiments described here. Another lamp spectrum under vacuum is included for comparison, showing the loss of intensity from absorption by air below ~190 nm. Lamp spectra are measured from 180 to 300 nm; spectra from 300 to 390 nm were obtained by extrapolation based on data provided by Oriel. The SO_2 absorption spectrum is from Wu et al. (2000) and Bogumil et al. (2003). Photodissociation threshold (219.2 nm, Okabe, 1978) is denoted by the dashed line; see text for details.

isotopes in products of both ^{18}O- and ^{16}O-rich SO_2 photolysis, in agreement with the fractionations observed in our experiments. However, the relative enrichments in ^{33}S, ^{34}S, and ^{36}S predicted by the model do not match the experimental data.

For the 25 Torr experiments, the model predicted positive values of $\Delta^{33}S$ and negative values of $\Delta^{36}S$ for both ^{16}O- and ^{18}O-rich SO_2, as we observed. Furthermore, the model predicted roughly similar enrichment in ^{33}S and ^{34}S, and slightly greater enrichment in ^{36}S, suggesting a significant contribution from shielding. The slightly lower enrichment predicted for ^{33}S and ^{34}S than for ^{36}S reflects the optically thick regimes for $^{33}SO_2$ and $^{34}SO_2$ at this pressure and reflects shielding of $^{33}SO_2$ and $^{34}SO_2$ as well as $^{32}SO_2$. These predictions were not consistent with experimental results, however, which showed progressively greater enrichment of ^{33}S, ^{34}S, and ^{36}S in elemental sulfur products using both $S^{18}O_2$ and SO_2. The magnitudes of $\Delta^{33}S$ and $\Delta^{36}S$ computed by the model were also consistently higher than what we observed. For the ^{18}O-rich case, the model predicted $\Delta^{33}S$ of 75.5‰ and $\Delta^{36}S$ of −141.5‰, compared with the average observed values of 13.25 ± 1.17‰ and −33.6 ± 1.37‰, respectively. The predicted $\Delta^{36}S/\Delta^{33}S$ was −1.9. For the ^{16}O-rich case, the model predicted $\Delta^{33}S$ of 76.4‰ and $\Delta^{36}S$ of −139.4‰, giving predicted $\Delta^{36}S/\Delta^{33}S$ of −1.8, compared to average observed values of 18.60 ± 2.62‰ and −43.47 ± 3.07‰ for $\Delta^{33}S$ and $\Delta^{36}S$. While in both cases the predicted values of $\Delta^{36}S/\Delta^{33}S$ were in rough qualitative agreement with the observed value of −2.4, neither case presented an exact match to the experiments. In addition, the model predicted approximately equal $\Delta^{33}S$ and $\Delta^{36}S$ magnitudes for $S^{18}O_2$ and SO_2, in contrast to our observations, which showed systematically reduced values for both $\Delta^{33}S$ and $\Delta^{36}S$ upon ^{18}O substitution.

For a pressure of 5 Torr, the model again predicted enrichment in all minor sulfur isotopes in photolytic products. The model implicated a role for shielding of $^{32}S^xO_2$, predicting approximately equal enrichments in ^{33}S and ^{34}S and slightly greater enrichment in ^{36}S for the ^{16}O-rich case. The modeled $\Delta^{36}S/\Delta^{33}S$ was −1.7 for SO_2, similar to predictions for the 25 Torr experiments. Experimental results at this pressure did not match these predictions, again showing progressively greater enrichment in ^{33}S, ^{34}S and ^{36}S. However, the slightly larger value of $\Delta^{33}S$ measured for the single 5 Torr experiment compared to the 25 Torr experiments is consistent with the absence of $^{33}SO_2$ shielding at the lower pressure. Unfortunately, due to the difficulty in obtaining yields of elemental sulfur product sufficient for isotopic analysis at low pressure, only a single experiment was performed at 5 Torr using ^{16}O-rich SO_2. No 5 Torr experiments were performed with ^{18}O-rich SO_2, so we are unable to compare experimental results for ^{16}O- and ^{18}O-rich SO_2 at low pressure.

4.3. Interpretation of experimental and modeling results

The observation of large S-MIF in product elemental sulfur implicates dissociation of SO_2 as a critical step in its formation. In our experiments, gas pressures of 5–25 Torr within the photocell yield a variable $^{32}SO_2$ column density of approximately 7×10^{18} to 4×10^{19} cm^{-2} and represent strongly shielding conditions for $^{32}SO_2$ (Lyons, 2007, 2009). In contrast, column densities for other isotopologues range from 1×10^{12} to 2×10^{18} cm^{-2}, with optical depths from ~2×10^{-5} to 20. The variations in optical depth among the isotopologues due to pressure differences between experiments present difficulties in attributing the experimental results solely to shielding, given the systematic variations in $\Delta^{33}S$ and $\Delta^{36}S$ between products of ^{16}O- versus ^{18}O-rich SO_2. Differences in peak-to-peak amplitudes and peak width for absorption spectra of different isotopologues reported by Danielache et al. (2008) also implicate a role for initial photoexcitation, and the existence of multiple pathways through which this dissociation could occur raises the possibility of a role for state-to-state transitions (Masterson et al., 2011).

Table 3a
Change in photodissociation rates ($J^yS^xO_2$) relative to $^{32}S^{16}O_2$ and $^{32}S^{18}O_2$ for no-opacity column, 5 and 25 Torr, and no lamp (integrated cross-section surface) cases (%).

	$S^{18}O_2$ enriched experiment			Natural SO_2 experiment		
	$J^{33}S^{18}O_2$	$J^{34}S^{18}O_2$	$J^{36}S^{18}O_2$	$J^{33}SO_2$	$J^{34}SO_2$	$J^{36}SO_2$
Integrated area	0.03	0.40	0.80	0.14	0.22	0.19
No shielding	0.47	1.14	2.13	0.23	0.41	0.61
5 Torr	3.48	4.09	5.21	3.26	3.36	3.68
25 Torr	16.22	16.54	18.24	16.09	15.79	16.66

Table 3b
Change in photodissociation enrichment factors relative to $^{32}S^{16}O_2$ and $^{32}S^{18}O_2$ for no-opacity column, 5 and 25 Torr, and no lamp (integrated cross-section surface) cases (%).

	$S^{18}O_2$ enriched experiment			Natural SO_2 experiment		
	$\varepsilon^{33}S^{18}O_2$	$\varepsilon^{34}S^{18}O_2$	$\varepsilon^{36}S^{18}O_2$	$\varepsilon^{33}SO_2$	$\varepsilon^{34}SO_2$	$\varepsilon^{36}SO_2$
Integrated area	0.30	4.04	7.94	1.41	2.21	1.94
No shielding	4.65	11.29	21.07	2.30	4.12	6.05
5 Torr	34.20	40.07	50.79	32.13	33.06	36.09
25 Torr	150.31	153.09	167.59	149.22	146.61	154.06

The observation here that substitution of ^{18}O for ^{16}O in the SO_2 significantly alters the magnitude of the S-MIF signal in elemental sulfur products provides an additional constraint that can be used to evaluate the potential roles of shielding, initial photoexcitation, and state-to-state transitions in the production of S-MIF during SO_2 photochemistry. We consider three hypotheses: a) different absorption by $S^{18}O_2$ and $S^{16}O_2$, b) state-to-state transitions, and c) redshifts in an optically thin atmosphere. If the explanation lies with differences in the absorption spectra of $S^{18}O_2$ and $S^{16}O_2$, as considered in the first hypothesis, then the spectra must shift in a way that implicates a specific change in the spectral structure, such as absorption peak height and/or width, with substitution of ^{18}O for ^{16}O in SO_2.

Although it is apparent that shielding occurred in these experiments, this effect alone cannot explain the observed isotopic composition of products. While the model successfully reproduced some attributes of the experimental data, it failed to account for the systematic variation in magnitude of $\Delta^{33}S$ and $\Delta^{36}S$ for $S^{18}O_2$ and SO_2. This suggests either that the variations in $\Delta^{33}S$ and $\Delta^{36}S$ for ^{16}O- versus ^{18}O-rich SO_2 cannot be explained simply by shielding or differential photoexcitation, at least within the limitations of our current model, or that the observed variations in S-MIF magnitude provide evidence for operation of another mechanism.

Other mechanisms for explaining the results of our experiments include a source of the observed fractionations that is linked to isotopologue-specific differences in light absorption and isotopologue-specific differences in the rates of state-to-state transformations leading to the reaction products. These mechanisms may be analogous to those inferred for S-isotopologues of CS_2 scaling with carbon substitution (Zmolek et al., 1999) and for O-isotopologues of CO_2 scaling with carbon substitution (Bhattacharya et al., 2000). Support for a role of differences in light absorption is provided by spectroscopic studies of Danielache et al. (2008, 2012) who document measurable differences in peak-to-valley amplitude and peak profiles for absorption profiles of the $^ySO_2$ isotopologues. Support for the second of these mechanisms is provided by Knappenberger and Castleman (2004), who saw an inverse kinetic isotope effect in excited state dynamics with substitution of ^{34}S for ^{32}S in gas-phase SO_2 experiments. They observed that excited states of $^{34}SO_2$ had slightly longer lifetimes than those of $^{32}SO_2$, implying greater probability of dissociation due to secondary processes for $^{34}SO_2$. Nelson and Borkman (1975) performed isotopic substitution experiments with solid-phase SO_2, finding that $S^{18}O_2$ displayed a longer phosphorescence lifetime for the $^3\tilde{B}_1$ state than $S^{16}O_2$. Both of these reports provide evidence that isotopic substitution within SO_2 isotopologues can alter the dynamics such that modified fractionation could manifest in photochemical products, and further suggest that the relative lifetimes of

excited molecular states may play a key role in defining the fractionation effects for various isotopologues.

Danielache et al. (2008) measured the UV absorption spectra of ^{16}O-rich $^{32}SO_2$, $^{33}SO_2$, and $^{34}SO_2$ and determined that red-shifting of spectral features for the heavier isotopologues alone could induce large enrichments of the minor sulfur isotopes in photolytic products, characterized by significantly mass-independent composition. To test the veracity of this hypothesis for oxygen isotope substitution in SO_2, we applied our model to estimate the predicted sulfur isotopic fractionation for the non-photon-limited case by evaluating the relative band intensities predicted due to differences in absorption spectra alone. The relative band intensities were computed from

$$\Omega_{x\_y\_x} = \frac{\int_{190}^{220} \sigma_{x\_y\_x}(\lambda)d\lambda - \int_{190}^{220} \sigma_{x\_32\_x}(\lambda)d\lambda}{\int_{190}^{220} \sigma_{x\_32\_x}(\lambda)d\lambda}, \quad (14)$$

where x = 16 or 18 and y = 33, 34, or 36. Subsequent fractionation factors were estimated using Eqs. (11) through (13), as before.

Results of these calculations are given in Tables 3a–3c. The model predicted enrichment in all minor sulfur isotopes due to differences in primary absorption among the isotopologues, with greater enrichments predicted for $S^{18}O_2$ than for SO_2. Interestingly, the model also predicted very different relationships between $\Delta^{33}S$ and $\Delta^{36}S$ upon oxygen isotope substitution, giving $\Delta^{36}S/\Delta^{33}S$ of 0.3 for $S^{18}O_2$ and −5.0 for SO_2.

Since these calculations assumed identical actinic flux for all isotopologues, the predicted isotopic fractionation is not reliant upon variations in optical depth among isotopologues, but instead depends upon differences in photochemical reaction rates that may be directly associated with primary photoexcitation or secondary selection processes associated with state-to-state transitions. While these calculations clearly do not attempt to replicate the conditions (pressure, temperature, and radiation spectrum) of the terrestrial and martian atmospheres, the support for a link to processes associated with photoexcitation and photodissociation in addition to the modification of photolytic radiation by shielding indicates that a mass-independent signal could be introduced through SO_2 photolysis in an optically thin atmosphere. This finding is relevant to models of the martian atmosphere, which may rely upon mechanisms presumed feasible for S-MIF production to constrain SO_2 abundance. It is important to note, however, that in a planetary atmosphere, pressure broadening will change the SO_2 linewidths, thereby changing the effect of shielding.

Fig. 3 shows a plot of $\Delta^{36}S$ versus $\Delta^{33}S$ for our experimental products and modeled results. Also shown are arrays representing average compositions measured in Archean sediments (Farquhar et al., 2000c) and in sulfate from the martian meteorites Nakhla and Lafayette (Farquhar et al., 2000c), indicating the diversity of S-MIF signals that have been observed in these different planetary environments. The figure highlights the prediction that similarly widespread variations in $\Delta^{36}S/\Delta^{33}S$ may be produced by primary photochemical processes due to differences in UV absorption spectra among the SO_2 isotopologues.

Table 3c
Change in photodissociation NMD factors relative to $^{32}S^{16}O_2$ and $^{32}S^{18}O_2$ for no-opacity column, 5 and 25 Torr, and no lamp (integrated cross-section surface) cases (‰).

	$S^{18}O_2$ enriched experiment		Natural SO_2 experiment	
	$\Delta^{33}S^{18}O_2$	$\Delta^{36}S^{18}O_2$	$\Delta^{33}SO_2$	$\Delta^{36}SO_2$
Integrated area	−1.8	0.2	0.3	−2.3
No shielding	−1.1	−0.5	0.2	−1.8
5 Torr	13.8	−26.7	15.2	−27.6
25 Torr	74.2	−143.2	76.2	−142.8

5. Conclusions

This report describes results of a suite of experiments designed to investigate the mechanism responsible for the observed S-MIF by comparing sulfur isotopic fractionation produced during the UV photolysis of ^{16}O-rich and ^{18}O-rich SO_2. Results of the experiments reveal generally reduced sulfur fractionation for ^{18}O-rich SO_2 as compared to ^{16}O-rich SO_2.

Modeling of our experiments using theoretically shifted absorption spectra suggests that while a S-MIF signature can be generated through isotopologue-specific absorption caused by red-shifting of spectral features associated with the strong bending mode progression that dominates the wavelength region from 180 to 220 nm, this cannot explain the difference between experiments with natural abundance SO_2 and $^{18}SO_2$. Evidently the explanation for this effect lies elsewhere, potentially with variations in excited-state dynamics of $S^{18}O_2$ and SO_2. Considering recent findings of Masterson et al. (2011) in conjunction with these data, the most parsimonious explanation for the observations implies a role for photophysical (absorption-related) and photochemical (related to rates of state-to-state transformations) effects in addition to shielding in the production of the observed S-MIF. It appears clear that differences in the absorption-related peak profiles (peak-to-valley) of $^{32}SO_2$, $^{33}SO_2$, $^{34}SO_2$, and $^{36}SO_2$ (c.f., Danielache et al., 2008, 2012) are instrumental in determining the relative fractionations of isotopologues. It also appears that further differences, possibly in the level of overlap between spectra for the sulfur isotopologues, may play a role in explaining the difference between the relative fractionations of SO_2 and $S^{18}O_2$. One photophysical difference that should be investigated further is a reduction in the peak-to-valley amplitude for the isotopologues of $^{18}SO_2$, possibly as a consequence of a lower density of rotational lines on ^{18}O substitution, which would result in greater overlap between spectra of the more-abundant and less-abundant isotopologues. This would reduce the magnitude of effects attributable to shielding and may allow for preservation of the relative differences between $\delta^{34}S$, $\Delta^{33}S$, and $\Delta^{36}S$.

Results of our modeling also indicate that red-shifting of spectral features for heavy isotopologues of SO_2 provides a mechanism for generating S-MIF that would be operable in optically thin regimes, relaxing constraints on atmospheric SO_2 column density required to produce S-MIF. This finding may be relevant to models of the martian atmosphere, given the differences in S-MIF characteristics observed in martian meteorites compared to Archean sediments. While our results suggest that it is possible to produce S-MIF signals regardless of SO_2 optical depth, the photochemistry occurring in planetary atmospheres may nonetheless involve multiple mechanisms.

A more rigorous treatment of this problem that incorporates more accurate details of spectral features, preferably using measured absorption spectra for each isotopologue, is warranted. In addition, it is suggested that future experiments designed to further investigate the sulfur isotopic fractionation occurring at low SO_2 pressures should be performed for longer durations to mitigate the difficulty in obtaining sufficient product yields for isotopic analysis.

Acknowledgments

The authors thank M. Quijada and T. Madison of NASA/GSFC for measurement of the D_2 lamp spectrum and J. Lyons, A. Pavlov, and R. Hudson for insightful discussions during the preparation of this manuscript. The authors also thank three reviewers and additional clarification by M. Johnson and S. Ono. J. F. acknowledges research support from the NASA Exobiology program. B.A.W. acknowledges support from the National Science and Engineering Research Council of Canada through the Discovery grants program.

Appendix A. Supplementary data

Supplementary data to this article can be found online at http://dx.doi.org/10.1016/j.chemgeo.2013.07.021.

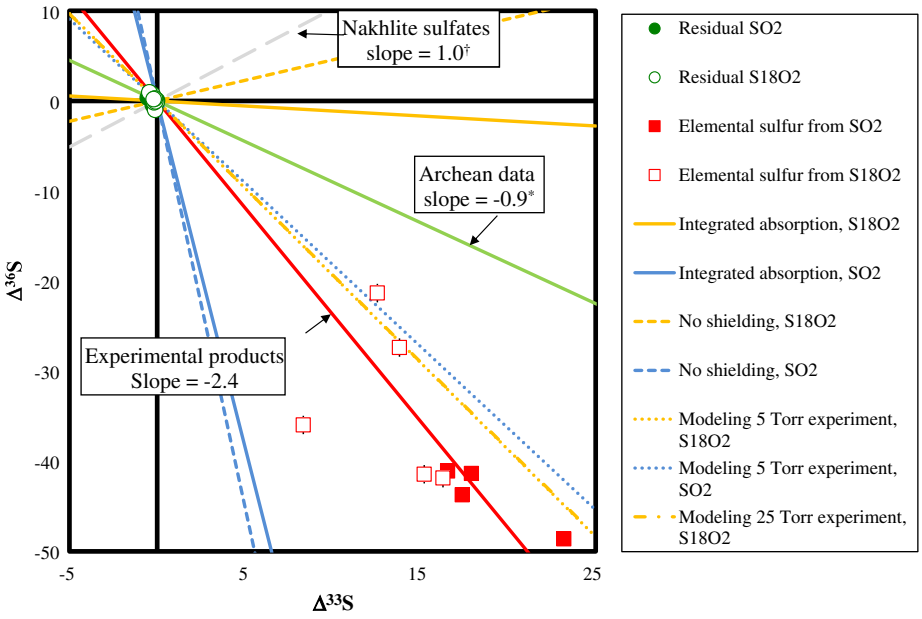

Fig. 3. Plot of $\Delta^{36}S$ vs. $\Delta^{33}S$ for products and residues of photolysis experiments, reported with respect to the initial gas composition. If 2σ error bars are not visible, they are smaller than the symbols. In the legend, "S18O2" indicates ^{18}O-rich SO_2, while "SO2" indicates ^{16}O-rich SO_2.
References: *Farquhar et al. (2001) and †Farquhar et al. (2000c, 2007a).

References

Archer, C.P., Elks, J.M., Western, C.M., 2000. The $C^3\Pi$, $d^1\Pi$, and $e^1\Pi$ states of SO. Journal of Chemical Physics 112, 6293–6300.

Bally, J., Langer, W.D., 1982. Isotope-selective photodestruction of carbon monoxide. The Astrophysical Journal 255, 143–148.

Bhattacharya, S.K., Savarino, J., Thiemens, M.H., 2000. A new class of oxygen isotopic fractionation in photodissociation of carbon dioxide: potential implication for atmospheres of Mars and Earth. Geophysical Research Letters 27, 1459–1462.

Bogumil, K., Orphal, J., Homann, T., Voigt, S., Spietz, P., Fleischmann, O.C., Vogel, A., Hartmann, M., Kromminga, H., Bovensmann, H., Frefick, J., Burrows, J.P., 2003. Measurements of molecular absorption spectra with the SCIAMACHY pre-flight model: instrument characterization and reference data for atmospheric remote-sensing in the 230–2380 nm region. Journal of Photochemistry and Photobiology A: Chemistry 157, 167–184.

Danielache, S.O., Eskebjerg, C., Johnson, M.S., Ueno, Y., Yoshida, N., 2008. High-precision spectroscopy of ^{32}S, ^{33}S, and ^{34}S sulfur dioxide: ultraviolet absorption cross sections and isotope effects. Journal of Geophysical Research 113. http://dx.doi.org/10.1029/2007JD009695.

Danielache, S.O., Hattori, S., Johnson, M.S., Ueno, Y., Nanbu, S., Yoshida, N., 2012. Photoabsorption cross-section measurements of ^{32}S, ^{33}S, ^{34}S, and ^{36}S sulfur dioxide for the B^1B_1–X^1A_1 absorption band. Journal of Geophysical Research-Atmospheres 117, D24301. http://dx.doi.org/10.1029/2012JD017464.

Farquhar, J., Bao, H., Thiemens, M.H., 2000a. Atmospheric influence of Earth's earliest sulfur cycle. Science 289, 756–758.

Farquhar, J., Savarino, J., Jackson, T.L., Thiemens, M.H., 2000b. A ^{33}S enrichment in ureilite meteorites: evidence for a nebular sulfur component. Geochimica et Cosmochimica Acta 64, 1819–1825.

Farquhar, J., Savarino, J., Jackson, T.L., Thiemens, M.H., 2000c. Evidence of atmospheric sulphur in the Martian regolith from sulphur isotopes in meteorites. Nature 404, 50–52.

Farquhar, J., Savarino, J., Airieau, S., Thiemens, M.H., 2001. Observation of wavelength-sensitive mass-independent sulfur isotope effects during SO_2 photolysis: implications for the early atmosphere. Journal of Geophysical Research 106 (E12), 32829–32839.

Farquhar, J., Kim, S.T., Masterson, A., 2007b. Implications from sulfur isotopes of the Nakhla meteorite for the origin of sulfate on Mars. Earth and Planetary Science Letters 264, 1–8.

Farquhar, J., Peters, M., Johnston, D.T., Strauss, H., Masterson, A., Wiechert, U., Kaufman, A.J., 2007a. Isotopic evidence for Mesoarchean anoxia and changing atmospheric sulfur chemistry. Nature 449, 706–710.

Freeman, D.E., Yoshino, K., Esmond, J.R., Parkinson, W.H., 1984. High-resolution absorption cross-section measurements of SO2 at 213 K in the wavelength region 172–240 nm. Planetary and Space Science 32, 239.

Halevy, I., Zuber, M., Schrag, D., 2007. A sulfur dioxide climate feedback on early Mars. Science 318, 1903–1907.

Holland, H.D., 2006. The oxygenation of the atmosphere and oceans. Philosophical Transactions of the Royal Society B 361, 903–915.

Johnson, S.S., Mischna, M.A., Zuber, M.T., Grove, T.L., 2008. Sulfur-induced greenhouse warming in early Mars. Journal of Geophysical Research 113. http://dx.doi.org/10.1029/2007JE002962.

Johnson, S.S., Pavlov, A.A., Mischna, M.A., 2009. Fate of SO_2 in the ancient martian atmosphere: implications for transient greenhouse warming. Journal of Geophysical Research 114. http://dx.doi.org/10.1029/2008JE003313.

Johnston, D.T., Puolton, S.W., Fralick, P.W., Wing, B.A., Canfield, D.E., Farquhar, J., 2006. Evolution of the oceanic sulfur cycle at the end of the Paleoproterozoic. Geochimica et Cosmochimica Acta 70, 5723–5739.

Knappenberger, K.L., Castleman, A.W., 2004. Photodissociation of sulfur dioxide: the E# state revisited. Journal of Physical Chemistry A 108, 9–14.

Lyons, J.R., 2007. Mass-independent fractionation of sulfur isotopes by isotope-selective photodissociation of SO_2. Geophysical Research Letters 28, 3231–3234.

Lyons, J.R., 2009. Atmospherically-derived mass-independent sulfur isotope signatures, and incorporation into sediments. Chemical Geology 267, 164–174.

Masterson, A.M., Farquhar, J., Wing, B.A., 2011. Sulfur mass-independent fractionation patterns in the broadband UV photolysis of sulfur dioxide: pressure and third body effects. Earth and Planetary Science Letters 306, 253–260.

Nelson, G.E., Borkman, R.F., 1975. Effect of oxygen-18 substitution upon electronic relaxation in the $^3B_1$ state of SO_2. Journal of Chemical Physics 63, 208–211.

Okabe, H., 1978. Photochemistry of Small Molecules. John Wiley, New York.

Postawko, S.E., Kuhn, W.R., 1986. Effect of the greenhouse gases (CO_2, H_2O, SO_2) on martian paleoclimate. Journal of Geophysical Research 91 (B4), D431–D438.

Ran, H., Xie, D., Guo, H., 2007. Theoretical studies of C^1B_2 absorption spectra of SO_2 isotopomers. Chemical Physics Letters 439, 280–283.

Savarino, J., Romero, A., Cole-Dai, J., Bekki, S., Thiemens, M.H., 2003. UV induced mass-independent sulfur isotope fractionation in stratospheric volcanic sulfate. Geophysical Research Letters 30, 2131. http://dx.doi.org/10.1029/2003GL018134.

Schmidt, J.A., Hattori, S., Yoshida, N., Nanbu, S., Johnson, M.S., Schinke, R., 2012. On the isotopic fingerprint exerted on carbonyl sulfide by the stratosphere. Atmospheric Chemistry and Physics Discuss 12, 25329–25353.

Schmidt, J.A., Johnson, M.S., Schinke, R., 2011. Isotope effects in N_2O photolysis from first principles. Atmos. Chem. Phys. 11 (17), 8965–8975.

Speth, R.S., Braatz, C., Tiemann, E., 1998. REMPI spectroscopy of SO singlet states. Journal of Molecular Spectroscopy 192, 69–74.

Thiemens, M.H., Heidenreich III, J.E., 1983. The mass-independent fractionation of oxygen: a novel effect and its possible cosmochemical implications. Science 219, 1073–1075.

Thiemens, M.H., Chakraborty, S., Dominguez, G., 2012. The physical chemistry of mass-independent isotope effects and their observation in nature. Annu. Rev. Phys. Chem. 63, 155–177.

Thode, H.G., Monster, J., Dunford, H.B., 1961. Sulphur isotope geochemistry. Geochimica et Cosmochimica Acta 25, 150–174.

Tian, F., Claire, M.W., Haqq-Misra, J.D., Smith, M., Crisp, D.C., Catling, D., Zahnle, K., Kasting, J.F., 2010. Photochemical and climate consequences of sulfur outgassing on early Mars. Earth and Planetary Science Letters 295, 412–418.

Tokue, I., Nanbu, S., 2010. Theoretical studies of absorption cross sections for the C^1B_2–X^1A_1 system of sulfur dioxide and isotope effects. Journal of Chemical Physics 132, 024301.

Ueno, Y., et al., 2009. Geological sulfur isotopes indicate elevated OCS in the Archean atmosphere, solving faint young sun paradox. Proceedings of the National Academy of Sciences of the United States of America 106 (35), 14784–14789.

Whitehill, A.R., Ono, S., 2012. Excitation band dependence of sulfur isotope mass-independent fractionation during photochemistry of sulfur dioxide using broadband light sources. Geochimica et Cosmochiica Acta 94, 238–253.

Wu, C.Y.R., Yang, B.W., Chen, F.Z., Judge, D.L., Caldwell, J., Trafton, L.M., 2000. Measurements of high-, room-, and low-temperature photoabsorption cross sections of SO_2 in the 2080- to 2950-Å region, with application to Io. Icarus 145, 289–296.

Xie, D., Guo, H., Bluský, O., Nachtigall, P., 2000. SO_2 (X^1A_1/C^1B_2) calculated from ab initio potential energy and transition dipole moment surfaces. Chemical Physics Letters 329, 503–510.

Zmolek, P., Xu, X., Jackson, T., Thiemens, M.H., Trogler, W.C., 1999. Large mass independent sulfur isotope fractionations during the photopolymerization of $^{12}CS_2$ and $^{13}CS_2$. Journal of Physical Chemistry 103, 2477–2480.